JACS
JOURNAL OF THE AMERICAN CHEMICAL SOCIETY
pubs.acs.org/JACS
Article

Catalytic Materials Enabled by a Programmable Assembly of Synthetic Polymers and Engineered Bacterial Spores

Masamu Kawada, Hyuna Jo, Alexis M. Medina, and Seunghyun Sim*

Cite This: J. Am. Chem. Soc. 2023, 145, 16210−16217
Read Online
ACCESS | Metrics & More | Article Recommendations | Supporting Information

ABSTRACT: Natural biological materials are formed by self-assembly processes and catalyze a myriad of reactions. Here, we report a programmable molecular assembly of designed synthetic polymers with engineered bacterial spores. This self-assembly process is driven by dynamic covalent bond formation on spore surface glycan and yields macroscopic materials that are structurally stable, self-healing, and recyclable. Molecular programming of polymer species shapes the physical properties of these materials while metabolically dormant spores allow for prolonged ambient storage. Incorporation of spores with genetically encoded functionalities enables operationally simple and repeated enzymatic catalysis. Our work combines molecular and genetic engineering to offer scalable and programmable synthesis of robust materials for sustainable biocatalysis.

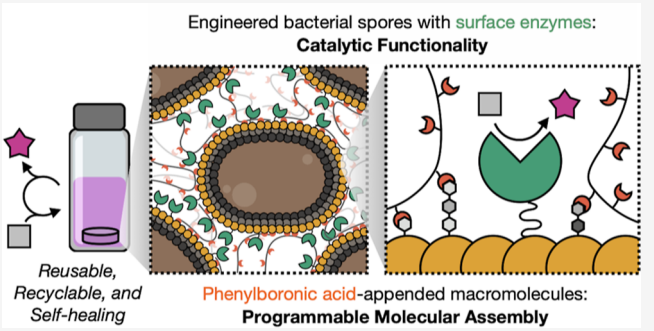

INTRODUCTION

Natural materials seamlessly integrate complex catalytic functionalities into a structural scaffold through an autonomous assembly process. The past few decades have seen the emergence of engineered living materials as a new way to capture biological functionalities.[1−3] Living cells in these materials were engineered to build biofilm-like structures or embedded into hydrogels to perform genetically-encoded enzymatic functions.[4−12] In addition, by combining rationally designed polymer scaffolds with genetically engineered cells, living materials can have tailored mechanical and dynamic properties. We have recently reported a molecular assembly strategy to construct living materials with designed synthetic polymers and living cells.[13,14]

One of the current limitations in living materials is that engineered cells require a continuous flow of energy (e.g., glucose and oxygen) and water to perform basic metabolism. Therefore, to realize the potential of living materials as a pragmatic and sustainable technology, their tendency toward functional death must be minimized. A spore-forming *Bacillus subtilis* brings unique solutions to this problem. It forms a dormant spore that is resilient against elevated temperatures, high osmolarity, UV radiation, and organic solvents.[15] A notable example of Voigt and co-workers' study examined the utility of *B. subtilis* spores by embedding them in molten agarose to create 3D-printable materials.[16] Living cells germinated from spores at the material surface could operate as biosensors and produce a pathogen-specific substance. While this spore-based approach significantly extends the material's shelf life compared to cell-based materials, the requisite germination step still limits its use outside of cell-friendly environments (i.e., nutrient-rich solutions). Meanwhile, we have recently demonstrated that *B. subtilis* spores can be engineered to act as tough and renewable catalyst particles that can perform repeated biocatalysis in both aqueous and organic solvents as well as in elevated temperatures.[17] T7 RNA polymerase-driven expression of recombinant proteins in sporulating cells resulted in high numbers of recombinant enzymes displayed on the spore surface. Because this approach allowed us to decouple enzymatic functionalities from cellular growth and survival, it motivated us to create catalytic spore-based materials for a sustainable biocatalysis platform allowing operational simplicity, dry storage, and reusability.

On the other hand, a well-defined molecular interface with macromolecular scaffolds is required to enable seamless integration of engineered spores into materials. We hypothesized that spore surface glycans could form dynamic covalent crosslinks with macromolecules bearing boronic acid handles. In our previous study, boronic acids have been shown to react with teichoic acid diols in bacterial cell walls and were harnessed as a reliable chemical handle for material synthesis.[14] Prior works in boronic acid-bearing polymers yielded self-healing hydrogels, glucose-responsive materials, and recyclable polymers through their reactivity toward diol and polyol

Received: May 17, 2023
Published: July 17, 2023

https://doi.org/10.1021/jacs.3c05153
J. Am. Chem. Soc. 2023, 145, 16210−16217

species.[18−21] Application of this dynamic covalent chemistry at the interface between macromolecules and engineered bacterial spores should therefore offer a powerful method to access functional spore-based materials with all the tunability and sustainability merits of abiotic dynamic covalent networks, such as self-healing, adaptiveness, and on-demand recycling.

Here we report the development of catalytic spore-based materials with modular mechanical and functional properties derived from the independent design and assembly of synthetic polymers and engineered spores (Figure 1). We discovered

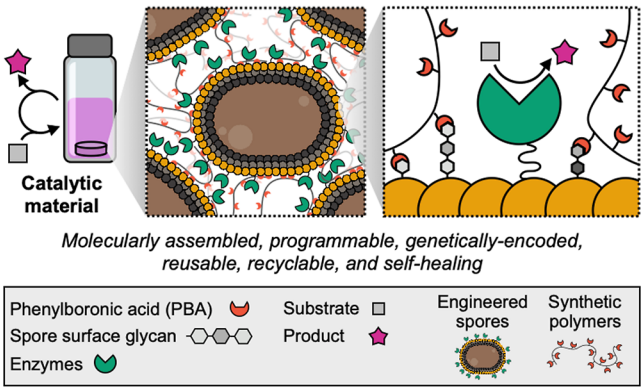

Figure 1. Schematic illustration of catalytic materials reported in this study. Programmable molecular assembly of synthetic polymers and genetically engineered bacterial spores resulted in macroscopic materials that exhibit robust biocatalytic activities, recyclability, and self-healing properties.

that phenylboronic acid (PBA) derivatives form tunable and reversible dynamic covalent bonds with the spore surface glycan. On the basis of this finding, PBA-functionalized statistical copolymers were assembled with *B. subtilis* to afford macroscopic materials that exhibited programmable stiffness, self-healing, dry storage, and recyclability. Integration of engineered spores yielded reusable biocatalytic materials with exceptional operational simplicity and high benchtop stability. The use of bacterial spores as an active partner in dynamic covalent crosslinking sets our material apart from previous examples and grants control over biocontainment as well as the subsequent fate of the spores through stimuli-responsive reversal of the crosslink.

RESULTS AND DISCUSSION

Programmable Dynamic Covalent Bond Formation at the *B. subtilis* Spore Surface. Crucial to the development of programmable spore-based materials is the molecular composition of the spore surface. The *B. subtilis* spore is formed by an asymmetric cell division event triggered under stress or nutrient-deprived conditions, and the resulting spore is reported to have surface glycan comprising glucose, galactose, and rhamnose.[22−25] To our knowledge, the exact structure of the spore glycan and, therefore, the quantity of available diols remains unknown. Nevertheless, we reasoned that a polysaccharide derived from glucose, galactose, and rhamnose should have abundant diols to react with boronic acids for covalent bond formation. The mechanism of boronic acid-diol condensation is solvent- and pH-dependent. In an aqueous solution, acid−base equilibrium constants (pK_a) of boronic acid species determine the composition of trigonal boronic acid and tetrahedral hydroxyboronate anion as well as their corresponding ester forms. Because the tetrahedral boronate ester has a higher equilibrium constant (K) than that of the trigonal boronic ester,[26] dynamic bond formation and reversal can be regulated as a function of the boron species' pK_a.

PBA has a phenyl ring that is usually conjugated with boron, and electron-withdrawing groups (EWGs) on the PBA can stabilize boron's negative charge buildup through resonance and polar effects.[26,27] We hypothesized that (1) diols on the spore glycan will react with PBAs to form stable covalent bonds and that (2) PBAs with EWGs will increase spore labeling by stabilizing the key negative charge on the boronate ester product. Spore labeling experiments were conducted using boronic acid probes to explore the programmability and reversibility of boronate ester linkages on *B. subtilis* (Figure 2a). We synthesized five different fluorescent PBA probes from 4-carboxyphenylboronic acid and its derivatives bearing various substituents at the meta position (Figures 2b and S2.1−S2.19). Ortho-substitutions to the boronic acid were avoided to minimize additional variables, such as steric strain, which could limit the desired π-conjugation.[28] Additionally, a control probe bearing tris(hydroxymethyl)aminomethane conjugated to sulfoCy5 (Tris-sCy5) instead of the PBA moiety was synthesized to observe the effect of PBAs independently from other spore-dye interactions (Figure S2.20).[14] These probes were incubated with *B. subtilis* spores in PBS buffer (10 μM, pH 7.16) for 20 h on a heating block at 30 °C and 800 rpm, and the spores were washed five times with PBS to rid of excess dyes. Fluorescence microscopy revealed no spore labeling from the control Tris-sCy5 probe while varying degrees of spore labeling were observed from the PBA probes (Figure 2c−h). The fluorescence intensities from these images followed the trend of $3NO_2$-PBA being the highest, followed by 3,5F-PBA, 3F-PBA, 3OMe-PBA, and PBA, in decreasing order (Figures 2c−h and S4.2). To quantitatively analyze this phenomenon, bulk fluorescence intensities were measured from labeled spore suspensions and normalized to account for spore concentration (OD_{600}) (Figures 2i and S4.2). The trend observed here corresponded well with the results from fluorescence images and suggests that aryl substituents with greater electron-withdrawing ability increase the overall spore labeling. Because diol structures, abundance, and compositions on spore surfaces are unknown, kinetic (k) and thermodynamic (K) parameters cannot be probed by spectroscopic methods such as NMR. Instead, we approximated relative K with normalized fluorescence because it directly shows the extent of bond formation on a spore surface. When plotted against the Hammett constant σ_{meta}, which quantifies the effect that meta substituents have on the ionization of groups directly attached to a benzene ring,[29] $\log(K)$ showed a positive correlation (Figure 2j). We also tested the charge-stabilization effect of the EWGs through pK_a measurements (Figure S5.1).[30] pK_a values for $3NO_2$-PBA, 3,5F-PBA, 3F-PBA, and PBA were determined to be 6.3, 7.0, 7.3, and 8.5, respectively. Strong correlations observed from plots of pK_a as a function of σ_{meta}, as well as $\log(K)$ as a function of pK_a, suggest that relative boronate ester formation on the spore can be predicted by both the aryl substituent constant and acidity of a PBA (Figure S5.2). We also conducted spore labeling studies in 98% methanol solutions to exploit the durability of *B. subtilis* spores in organic solvents.[17] Similar trends with lower overall spore labeling indicated that the programmable PBA-spore binding is not limited to purely aqueous conditions (Figure S4.3).

https://doi.org/10.1021/jacs.3c05153
J. Am. Chem. Soc. 2023, 145, 16210−16217

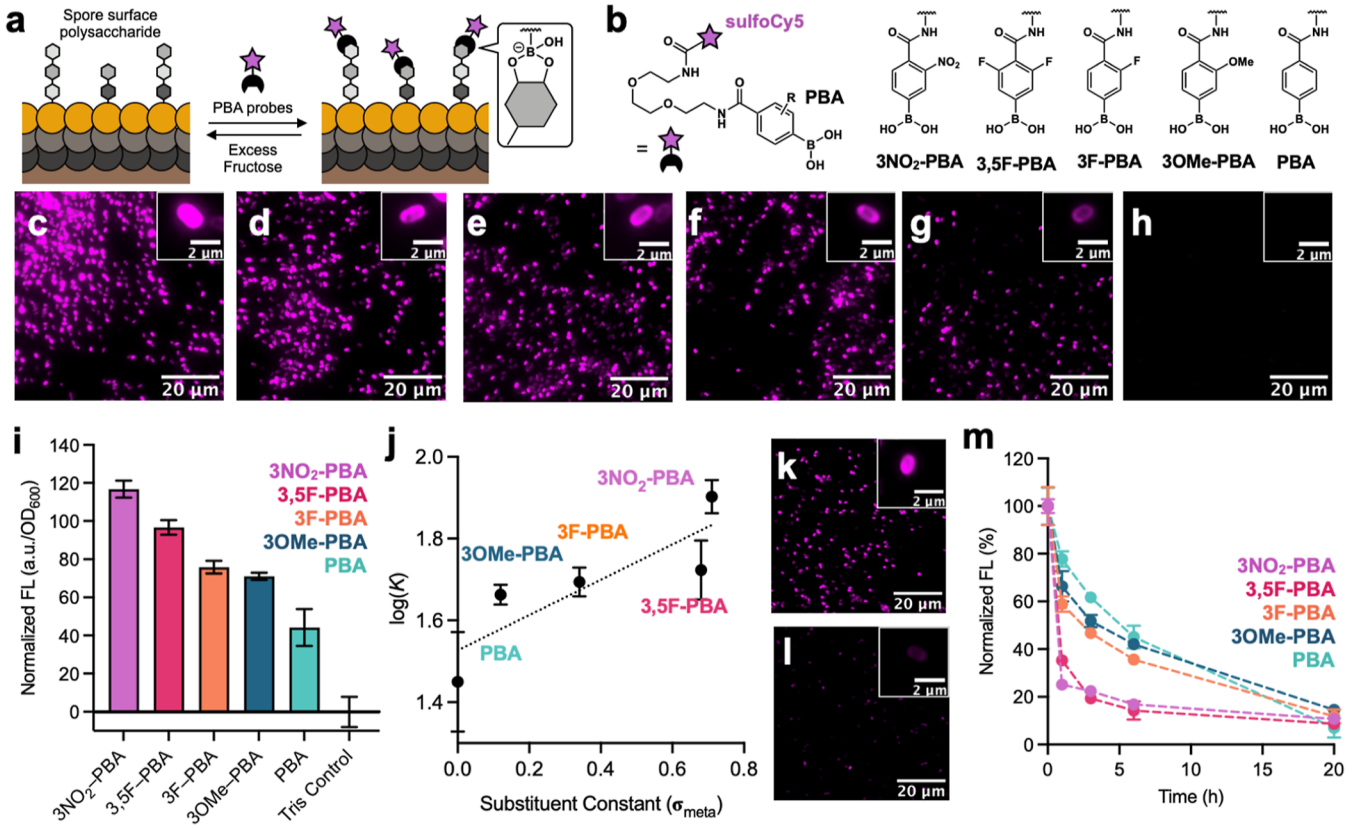

Figure 2. Programmable dynamic covalent bond formation at the *B. subtilis* spore surface. (a) Schematic illustration of spore labeling via boronate ester bond formation between spore surface glycan and fluorescent PBA probes. (b) Molecular structures of five fluorescent PBA probes with varying aryl substituents. (c–h) Representative fluorescence microscopy images of labeled spores with (c) $3NO_2$-PBA, (d) 3,5F-PBA, (e) 3F-PBA, (f) 3OMe-PBA, (g) PBA, and (h) control probe Tris-sCy5. (i) Normalized bulk fluorescence emission of labeled spore suspensions prepared by incubating each fluorescent probe with spores and subsequent washing. (j) Correlation between relative equilibrium constant K from spore labeling experiments and Hammett constants σ_{meta}. (k,l) Representative fluorescence microscopy images of labeled spores with 3,5F-PBA probe (k) before and (l) 20 h after fructose addition. (m) Normalized fluorescence intensities of the labeled spore suspensions incubated with 50 mM fructose over time. Samples were washed with PBS before measurements. Studies conducted in phosphate buffer saline (PBS).

The reversibility of boronate ester-mediated dynamic covalent bonds on the spore surface was investigated in aqueous conditions using a competing diol species, fructose. A visible decrease in spore labeling from fluorescence microscopy was observed over 20 h (Figures 2k,l and S4.4). A kinetic plot of the normalized fluorescence intensity over time showed that more acidic PBAs show faster bond reversibility (Figure 2m). The trend is consistent with diol exchange reaction kinetics with fructose that is accelerated by the charge-stabilizing effects from EWGs. Altogether, these results confirm our hypothesis and establish the basis for designing programmable molecular assemblies involving *B. subtilis* spores.

Molecularly Programmed Material Assembly of *B. subtilis* Spores and PBA-Appended Statistical Copolymers. Based on the small molecule study, we envisioned a programmable assembly of *B. subtilis* spores and PBA-functionalized synthetic polymers. Statistical copolymers were designed to include a 2-aminoethyl methacrylate (AEMA) monomer that can undergo post-polymerization modification to append various PBAs at the terminal amine (Figures S2.21 and S2.22). Polymer solubility was largely dependent on the comonomer identity, and we found that copolymers derived from 2-hydroxyethyl methacrylate (HEMA) and di(ethylene glycol) methyl ether methacrylate (DEGMEMA) consistently dissolved in methanol at high concentrations. Free radical polymerization between AEMA and a comonomer followed by EDC coupling with 4-carboxyPBAs afforded functionalized statistical copolymers at gram scales (Figures S2.26–S2.31). The percentage of PBA in a polymer chain was maintained at 9–10% for all copolymers. Reversible addition-fragmentation chain transfer (RAFT) polymerization was employed to afford narrow-dispersity polymers (Figures S2.23–S2.25 and S2.32–S2.34). All polymer species used in this study are summarized in Table S1.

Assembly of synthetic copolymers and *B. subtilis* spores afforded a macroscopic hydrogel (Figure 3a). The material was made by mixing 50 μL of concentrated spores in water with 100 μL of a 33 w/v % polymer solution in methanol (Video S1). We note that polymer solutions themselves are liquids, and only when spores are added a self-standing hydrogel is formed (Figure 3b). This highlights that our material is distinct from other examples of spore-embedding hydrogels where a polymer network is independently formed without spores.[16] In these spore-polymer hybrid materials, spores serve as cross-linking points and are crucial for the molecular assembly of materials. These materials are self-standing and stable even when immersed in water (Figure 3c). We also found that macroscopic material assembly is possible using a different comonomer as long as the polymer exhibits high solubility and the essential PBA motif is present to facilitate the spore-polymer crosslinking (Figure S10).

https://doi.org/10.1021/jacs.3c05153
J. Am. Chem. Soc. 2023, 145, 16210–16217

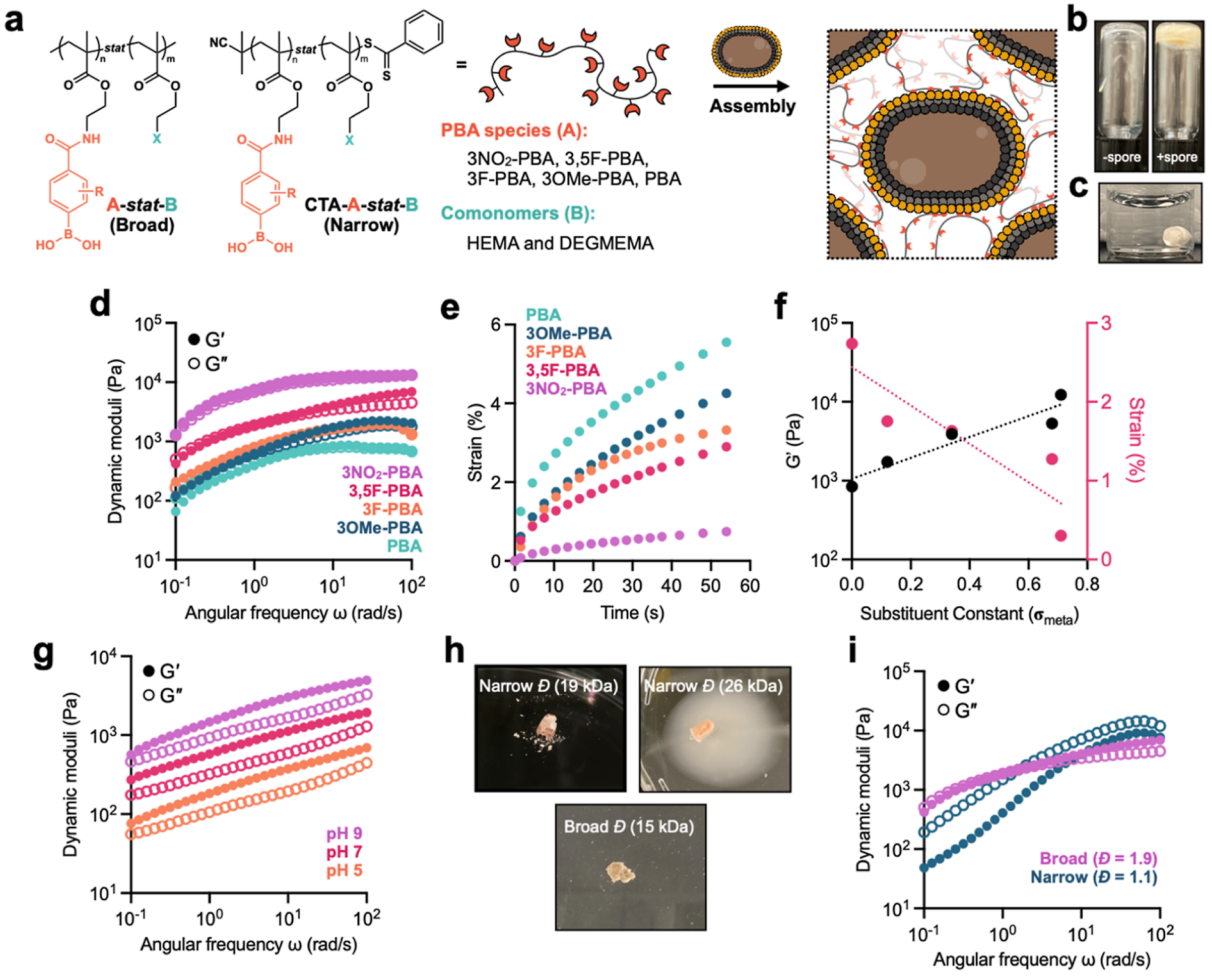

Figure 3. Molecularly programmed material assembly of *B. subtilis* spores and PBA-appended statistical copolymers. (a) Schematic illustration of PBA-functionalized statistical copolymers assembled with *B. subtilis* spores to afford (b) self-standing hydrogels that (c) maintain their structural integrity under water. Importantly, without spores, polymers do not form hydrogels. (d) Storage moduli G' and loss moduli G'' at 25 °C of assembled materials with statistical copolymers prepared with HEMA comonomer and conjugated with various PBA species. (e) Percentage of deformation of materials with varying conjugated PBA species under constant stress. (f) A correlation plot of the storage moduli at 10 rad/s and creep strain at 10 s against substituent Hammett constants of different PBAs. (g) pH-dependent storage moduli G' and loss moduli G'' of assembled materials with copolymers conjugated with 3,5F-PBA. (h) Optical images of assembled materials dried and subsequently submerged in water. These materials were prepared using copolymers with broad $Đ$ copolymers (15 kDa) or narrow $Đ$ copolymers of different molecular weights (19 or 26 kDa). (i) Storage moduli G' and loss moduli G'' of assembled materials comprising broad or narrow $Đ$ copolymers conjugated with 3,5F-PBA.

Time-dependent viscoelastic properties of these materials were probed with shear rheology at 25 °C (Figure 3d). The storage modulus (G') of $3NO_2$-PBA was the highest over the entire frequency region, followed by other PBA derivatives with a general trend of 3,5F-PBA, 3OMe-PBA, 3F-PBA, and PBA in decreasing order, suggesting that the charge-stabilizing effect of EWGs increases material stiffness by encouraging the formation of boronate ester crosslinks. We performed a creep test on these hydrogels and measured the percentage of deformation over time with constant stress (Figure 3e). Resistance to deformation also mirrored the trend shown in shear rheology. We plotted the storage modulus (G') at a fixed frequency (10 rad/s) and the percentage strain at a fixed time point (10 s) against Hammett constants σ_{meta} (Figure 3f). A positive correlation between σ_{meta} and G', as well as a negative correlation between σ_{meta} and the amount of deformation, clearly shows that EWG-mediated negative charge stabilization determines the crosslinking density of these materials. In addition, the dynamic moduli of these materials increased as the pH was increased (Figure 3g), demonstrating that stimuli-induced ionization of the boron species also changes the crosslinking density. Taken together, PBA-diol crosslinking density, which is controlled by the charge stabilization effect of EWGs, programs the mechanical properties of these macroscopically assembled hybrid materials. We decided to use the 3,5F-PBA polymer as a model polymer for further studies on material properties due to its relative ease in both synthesis and characterization.

Strikingly, the dispersity ($Đ$) of copolymer species significantly impacts spore containment and viscoelastic behaviors. While both narrow (19 kDa) and broad (15 kDa) $Đ$ polymers of a similar size yield an assembly of materials with spores, the narrow $Đ$ sample became brittle upon drying (Figure 3h). Rheological measurements of the hydrated materials showed that the narrow $Đ$ material exhibits a more liquid-like behavior where G' was smaller than the loss moduli (G''), and the broad $Đ$ material was a viscoelastic solid with G' mostly greater than G'' (Figure 3i). Higher-molecular weight

https://doi.org/10.1021/jacs.3c05153
J. Am. Chem. Soc. 2023, 145, 16210−16217

(26 kDa) narrow $Đ$ polymers afforded stable materials even after drying but resulted in spore leaking (Figure 3h). We conducted a rheological study on materials comprising narrow $Đ$ polymers in various molecular weights and found that the material made from 19 kDa polymers possessed a dramatic frequency-dependent stiffening property while samples containing polymers of 26- and 57 kDa presented frequency-independent shear moduli (Figure S11). The gradual frequency-dependent stiffness observed in the broad $Đ$ samples (Figure 3d) appeared to result from a combination of low and high molecular-weight polymers. Therefore, the enhanced material stiffness, structural integrity, and biocontainment ability of the broad $Đ$ samples seem to arise from a synergistic effect between polymer chains of varying lengths that hold together the microstructures within the material, causing a space-filling effect.

Stimuli-Responsive Bond Restructuring Mechanism of the Molecular Assembly Enables Stable, Self-Healing, and Recyclable Materials. A molecularly assembled material equipped with a bond restructuring mechanism involving durable spores would yield benchtop stability, self-healing ability, and recyclability (Figure 4a). One of the major limitations of cell-based materials is that biological functions are inherently tied to cellular viability, which requires a flow of water and energy sources at all times. Because spores bypass this requirement, our spore-based materials can be stored under ambient and static conditions, even in a dried form (Figure 4b). When dried, these materials exhibited a Young's modulus of 1.6 MPa on average (Figure S6.1). Rehydrating these dried materials in water recovers their original shapes (Figure 4b) and increases their overall stiffness (Figure S6.2). A drying event likely prompts a shift in equilibrium towards an increased number of crosslinks because the gradual expulsion of water molecules from the local environment drives forward the key condensation reaction.

We investigated the boronate ester bond reversibility at the macroscopic scale by taking rheological measurements before and after a self-healing event. Pristine bulk materials were completely cut into two pieces and placed back together in contact (Figure 4c). They underwent macroscopic self-healing in under 30 min in both ambient and underwater conditions (Figures 4c and S7). The restored materials showed no evidence of mechanical damage at the first fracture site when stretched after healing (Figures 4d and S7). Rheological measurements of these materials also showed a complete recovery of their original viscoelastic properties (Figures 4e and S7).

Because the interaction between PBAs and spore surface glycan can be disturbed by adding competing diol species, such as fructose (Figure 2m), we set out to explore the recyclability of our materials. When immersed in an aqueous fructose solution (50 mM, 250 rpm, 37 °C), visible material disassembly was observed over 12 h with increasing solution turbidity (Figures 4f and S8.1). Disassembled polymer and spores were separated by centrifugation, and the obtained polymer solution was dialyzed against a saturated ammonium chloride solution. The recovered copolymer was spectroscopically identical to the pristine ones (Figure 4g) and was obtained as a powder with quantitative recovery (Figure S8.2). We demonstrated that a new batch of assembled materials, which shows similar viscoelastic properties to the pristine materials, could be produced with recycled copolymers (Figure S8.3).

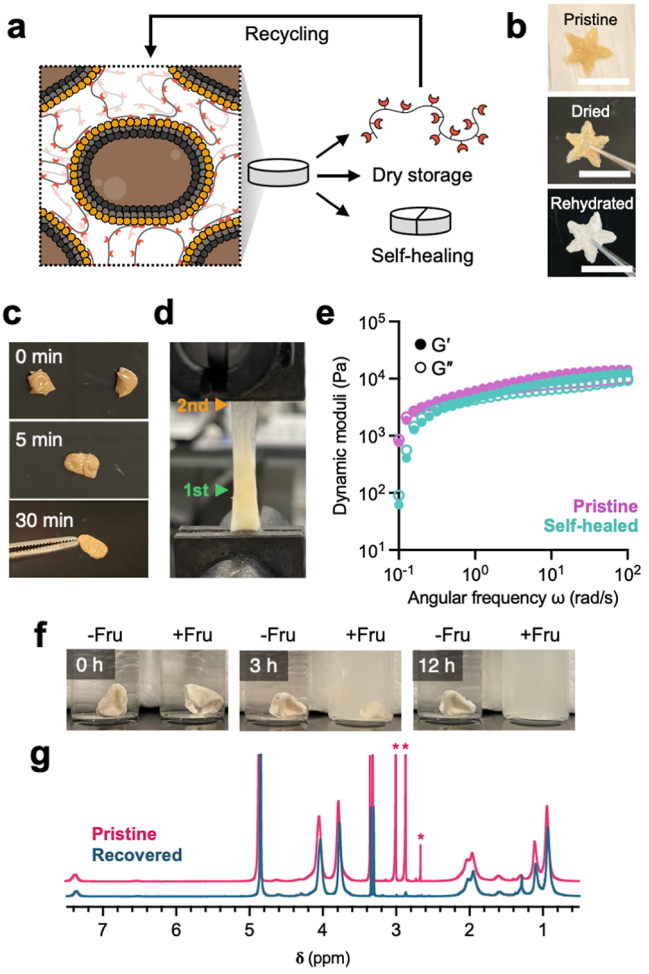

Figure 4. Stimuli-responsive bond restructuring mechanism of the molecular assembly enables stable, self-healing, and recyclable materials. (a) Schematic illustration of material properties arising from the dynamic covalent interface between spores and synthetic polymers. (b) Representative optical images of a pristine material (top), material after dehydration (middle), and material after subsequent rehydration in water (bottom). (c) Demonstration of self-healing event. Materials were completely cut into two and placed back together for 30 min. (d) Stretching a self-healed material. The first fracture site prior to a healing event is indicated with green triangle, and the second fracture site is indicated with orange triangle. (e) Storage moduli G' and loss moduli G'' of assembled materials before and after a self-healing event. (f) Optical images of materials immersed in 50 mM fructose (PBS) at 37 °C for 12 h (g) NMR overlay of the original and recovered copolymer. The asterisks at 2.99 and 2.86 ppm correspond to methyl peaks from residual DMF and the asterisk at 2.65 ppm correspond to a methyl peak from residual DMSO.

Catalytic Materials Enabled by a Molecular Assembly of Synthetic Polymers with Engineered *B. subtilis* Spores. Enzymes possess high selectivity and efficiency in mild conditions but have limited use in organic syntheses due to their notorious fragility, difficulty in separation from reaction mixtures, and limited scalability and reusability.[31,32] We have previously developed the T7 RNA polymerase-enabled high-density enzyme display (TIED) to express an enzyme of interest onto the surface of *B. subtilis* spores, catalyzing reactions that are both native and non-native to the bacteria.[17] This platform allows us to (re-)use enzymes without protein synthesis, isolation, or immobilization. We anticipated

https://doi.org/10.1021/jacs.3c05153
J. Am. Chem. Soc. 2023, 145, 16210−16217

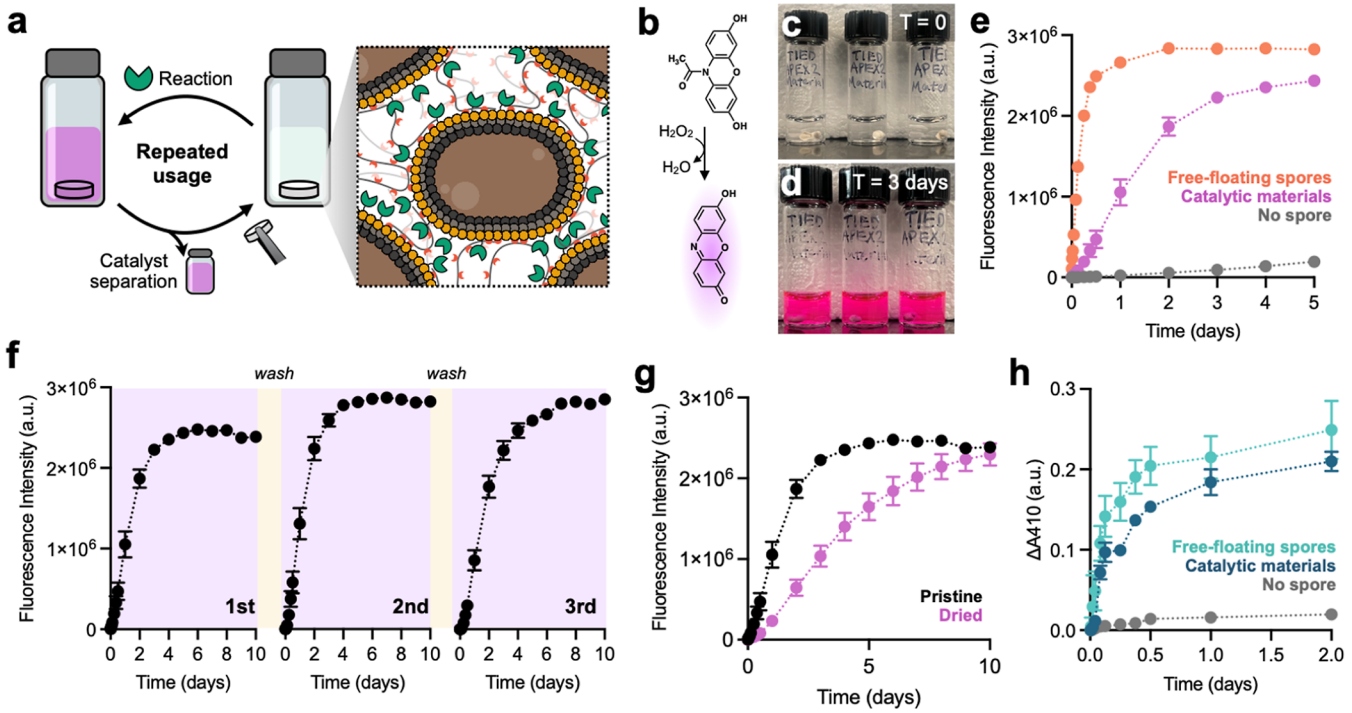

Figure 5. Catalytic materials enabled by a molecular assembly of synthetic polymers with engineered *B. subtilis* spores. (a) Schematic illustration of reusable catalytic materials enabled by the molecular assembly of polymers with engineered spores. (b) Schematic illustration of the APEX2-catalyzed conversion of Amplex Red to colorogenic and fluorogenic product, resorufin. (c,d) Optical images showing materials performing APEX2-catalyzed reaction in PBS (c) immediately after the start and (d) after 3 days. (e) Resorufin production probed by bulk fluorescence emission over time in samples containing catalytic materials, free-floating engineered spores, and no spores. (f) Reuse of materials catalyzing the conversion of Amplex Red to resorufin in three consecutive reaction cycles. (g) Resorufin production probed by bulk fluorescence emission over time in samples containing pristine catalytic materials and materials stored to dryness over 2 days. (h) Catalytic materials prepared with lipase-displaying spores catalyzing the conversion of *p*-nitrophenyl palmitate to *p*-nitrophenol in a tris buffer (50 mM, pH 8.0).

that integration of these engineered spores into our molecular assembly would yield catalytic materials with remarkable operational simplicity and reusability at a macroscopic scale (Figure 5a). A reaction can be (re-)initiated by introducing this material into a reaction mixture, and removed once the reaction is complete.

We set out to synthesize and test the performance of catalytic materials assembled with engineered spores from our previous study.[17] APEX2, an ascorbate peroxidase that can catalyze the conversion of Amplex Red into colorogenic and fluorescent resorufin (Figure 5b), was displayed on the *B. subtilis* spore surface and incorporated into material assembly (Figure 5c). The material was placed into a PBS solution (pH 7.2, 37 °C, 250 rpm) containing Amplex Red (0.1 mM) and hydrogen peroxide (0.8 mM), a cofactor for this reaction. Over time, the product formation was visible from its intense pink color and fluorescence emission in the solution (Figures 5d and S9.1.1). Meanwhile, immersed materials were completely intact. We evaluated the kinetics of the product formation via bulk fluorescence emission of the solution (Figure 5e). While the free-floating engineered spores exhibited the fastest catalysis, catalytic materials encasing these spores exhibited comparable conversion. Limited diffusion of the substrate into the materials may be the reason for the observed delay. Furthermore, these materials could be reused at least two more times by simply removing them from the reaction mixture, washing them, and placing them into a new reaction mixture (Figures 5f and S9.1.2–S9.1.4). During these three consecutive cycles, we did not observe any decrement in their catalytic activity. They also retained their catalytic ability after prolonged dry benchtop storage, albeit at a slower rate (Figures 5g and S9.1.7). Reaction kinetics could be affected by greater crosslink density and thus smaller pore sizes that permit less of the Amplex Red to pass through, which is consistent with the observed increase in material stiffness after drying and rehydration (Figure S6.2). The materials were also structurally intact with no sign of spore leakage, highlighting their exceptional stability and durability (Figure S9.1.1–S9.1.7). Material disassembly (Figure 4f) followed by a sequence of spore recovery, germination, culture, and sporulation afforded all-new spores with fully recovered catalytic activity (Figure S12).

We also incorporated lipase-displaying spores into the assembly of materials and tested their catalytic activity. The material was placed into a tris solution (pH 8.0, 37 °C, 250 rpm) containing *p*-nitrophenyl palmitate (0.1 mM), which produces colorogenic *p*-nitrophenol as a reaction product. Analogous to the materials made with APEX2-displaying spores, similar catalytic conversions were observed in free-floating spores and assembled materials, with faster catalytic activity from free-floating spores (Figure 5h). Interestingly, we observed spore leakage characterized by increases in visible solution turbidity and in OD_{600} measurements after 2 days (Figure S9.2.1). Storing the material to dryness made neither a significant difference to the catalysis nor the spore leakage (Figure S9.2.4). Since this biocontainment issue was not observed in our other materials, we considered the enzyme identity and solution pH as possible causes. The lipase-catalyzed production of *p*-nitrophenol involves ester cleavage and the production of an acid byproduct, both of which could

https://doi.org/10.1021/jacs.3c05153
J. Am. Chem. Soc. 2023, 145, 16210–16217

affect spore-polymer crosslinking either by polymer degradation or by a shift in boronate ester formation equilibrium. The final pH of the reaction solution remained at 8.0 and spore leaking was not observed at a lower pH (7.2 in PBS) (Figure S9.2.6). On the other hand, a ^{1}H NMR spectrum of the supernatant after 10 days of biocatalysis revealed peaks correlating to degraded polymer fragments (Figure S9.2.5). NMR from retrieved copolymers from these samples after complete disassembly via fructose treatment further revealed that approximately 20% of the PBA motif was lost during the hydrolysis reaction (Figure S9.2.5). It therefore seems likely that the ester linkages in the side chain were cleaved by displayed lipases on the spore surface. This result emphasizes that catalytic functionalities of enzymes should be taken into consideration in the designs of polymers and hints at the possibility of self-degrading materials when the appropriate spore, polymer, and solvent are combined.

One of the exciting features of the spore-based enzyme display system is the renewability of the enzymatic function by germinating cells from dormant spores and subsequently inducing sporulation to yield a new batch of catalytic spores (Figure S12).[17] When combined with the complete recyclability of the polymeric component in this assembly (Figures 4g and S8.2 and S8.3), we envision a sustainable biocatalysis platform featuring recycling and renewal of both components. The end users of these materials will be able to store them in ambient conditions, use them multiple times, and when the enzymatic activity decreases, reproduce catalytic materials on demand.

CONCLUSIONS AND OUTLOOK

This work reports molecularly programmable, recyclable, self-healing, and reusable catalytic materials formed via self-assembly of PBA-appended copolymers with engineered spores. We showed that binding affinities of PBA derivatives to spore surface glycan are controlled by aryl substituent effects. Gratifyingly, these tunable molecular interactions shape the mechanical properties of assembled materials. In addition, we showed the effect of polymer dispersity on the mechanical and spore-containing properties of these assemblies. The bond restructuring mechanism at the spore-polymer interface and the inherent durability of dormant spores together result in self-healing, ambient dry storage, and recycling of materials. Finally, materials containing engineered spores perform biocatalysis for multiple consecutive cycles without loss in activity.

Our biocatalysis platform presents a new direction for the practical synthesis of robust materials equipped with catalytic functionalities. Utilizing genetically engineered spores instead of purified enzymes brings significant advantages in scalability, production cost, reusability, and regeneration of catalytic functions. Further, the molecular assembly of spore particles into macroscopic materials with designed polymers enables exceptionally simple operation for biocatalytic reactions. Independent control for polymers and spores will create a vast array of combinations and enable the design of custom materials with specific functionalities, solvent compatibility, and mechanical properties. In this regard, this work opens a new chapter for marrying high-performance polymeric materials with durable biocatalytic functionality, which will find its utility beyond laboratory research.

ASSOCIATED CONTENT

Supporting Information

The Supporting Information is available free of charge at https://pubs.acs.org/doi/10.1021/jacs.3c05153.The data generated in this study are archived at the Dryad Repository: https://doi.org/10.7280/D1611W.

Supporting Information Video 1: A representative video visualizing the material synthesis process (MOV)

Materials, instrumentations, experimental and synthetic methods, ^{1}H, ^{13}C, and ^{1}H−^{1}H COSY NMR spectra, HRMS and MALDI-TOF data, gel permeation chromatography measurements, fluorescence microscopy and spectroscopy results, UV−vis spectrophotometric acid-base titration curves, pK_a correlation plots, nanoindentation measurements, rheological characterization, tensile testing, OD_{600} and OD_{410} measurements, optical images of materials and reaction mixtures (PDF)

AUTHOR INFORMATION

Corresponding Author

Seunghyun Sim − *Department of Chemistry, University of California Irvine, Irvine, California 92697, United States; Department of Chemical and Biomolecular Engineering, Department of Biomedical Engineering, and Center for Complex and Active Materials, University of California Irvine, Irvine, California 92697, United States;* orcid.org/0000-0002-4232-5917; Email: s.sim@uci.edu

Authors

Masamu Kawada − *Department of Chemistry, University of California Irvine, Irvine, California 92697, United States;* orcid.org/0000-0001-5016-6322

Hyuna Jo − *Department of Chemistry, University of California Irvine, Irvine, California 92697, United States*

Alexis M. Medina − *Department of Chemistry, University of California Irvine, Irvine, California 92697, United States*

Complete contact information is available at: https://pubs.acs.org/10.1021/jacs.3c05153

Author Contributions

The manuscript was written through contributions of all authors, and all authors have given approval to the final version of the manuscript.

Notes

The authors declare no competing financial interest.

ACKNOWLEDGMENTS

This work is supported by the National Science Foundation CAREER Award (DMR-2237344), UC Irvine Start-up, and partial support from the NSF Materials Research Science and Engineering Center program through the UC Irvine Center for Complex and Active Materials (DMR-2011967). The authors acknowledge the use of facilities and instrumentation at the UC Irvine Materials Research Institute (IMRI) supported in part by the National Science Foundation Materials Research Science and Engineering Center program through the UC Irvine Center for Complex and Active Materials (DMR-2011967). M.K. acknowledges support from the Department of Defense through the National Defense Science & Engineering Graduate (NDSEG) fellowship. A.M.M. was supported by Allergan undergraduate research fellowship, UROP, and SURP fellowships from UC Irvine. Nuclear Magnetic Resonance

measurements were performed in the NMR facility in the Department of Chemistry, UC Irvine.

REFERENCES

(1) Gilbert, C.; Ellis, T. Biological engineered living materials: growing functional materials with genetically programmable properties. *ACS Synth. Biol.* **2018**, *8*, 1−15.
(2) Nguyen, P. Q.; Courchesne, N. M. D.; Duraj-Thatte, A.; Praveschotinunt, P.; Joshi, N. S. Engineered living materials: prospects and challenges for using biological systems to direct the assembly of smart materials. *Adv. Mater.* **2018**, *30*, 1704847.
(3) Srubar, W. V., III Engineered living materials: taxonomies and emerging trends. *Trends Biotechnol.* **2021**, *39*, 574−583.
(4) Duraj-Thatte, A. M.; Manjula-Basavanna, A.; Courchesne, N.-M. D.; Cannici, G. I.; Sánchez-Ferrer, A.; Frank, B. P.; van't Hag, L.; Cotts, S. K.; Fairbrother, D. H.; Mezzenga, R.; et al. Water-processable, biodegradable and coatable aquaplastic from engineered biofilms. *Nat. Chem. Biol.* **2021**, *17*, 732−738.
(5) Duraj-Thatte, A. M.; Courchesne, N. M. D.; Praveschotinunt, P.; Rutledge, J.; Lee, Y.; Karp, J. M.; Joshi, N. S. Genetically programmable self-regenerating bacterial hydrogels. *Adv. Mater.* **2019**, *31*, 1901826.
(6) Huang, J.; Liu, S.; Zhang, C.; Wang, X.; Pu, J.; Ba, F.; Xue, S.; Ye, H.; Zhao, T.; Li, K.; et al. Programmable and printable Bacillus subtilis biofilms as engineered living materials. *Nat. Chem. Biol.* **2019**, *15*, 34−41.
(7) Nguyen, P. Q.; Botyanszki, Z.; Tay, P. K. R.; Joshi, N. S. Programmable biofilm-based materials from engineered curli nanofibres. *Nat. Commun.* **2014**, *5*, 4945.
(8) Zhang, C.; Huang, J.; Zhang, J.; Liu, S.; Cui, M.; An, B.; Wang, X.; Pu, J.; Zhao, T.; Fan, C.; et al. Engineered Bacillus subtilis biofilms as living glues. *Mater. Today* **2019**, *28*, 40−48.
(9) Chen, A. Y.; Deng, Z.; Billings, A. N.; Seker, U. O.; Lu, M. Y.; Citorik, R. J.; Zakeri, B.; Lu, T. K. Synthesis and patterning of tunable multiscale materials with engineered cells. *Nat. Mater.* **2014**, *13*, 515−523.
(10) Wang, Y.; An, B.; Xue, B.; Pu, J.; Zhang, X.; Huang, Y.; Yu, Y.; Cao, Y.; Zhong, C. Living materials fabricated via gradient mineralization of light-inducible biofilms. *Nat. Chem. Biol.* **2021**, *17*, 351−359.
(11) Liu, X.; Inda, M. E.; Lai, Y.; Lu, T. K.; Zhao, X. Engineered living hydrogels. *Adv. Mater.* **2022**, *34*, 2201326.
(12) Murphy, R. D.; Garcia, R. V.; Oh, S. J.; Wood, T. J.; Jo, K. D.; Read de Alaniz, J.; Perkins, E.; Hawker, C. J. Tailored Polypeptide Star Copolymers for 3D Printing of Bacterial Composites Via Direct Ink Writing. *Adv. Mater.* **2023**, *35*, 2207542.
(13) Jo, H.; Selmani, S.; Guan, Z.; Sim, S. Sugar-Fueled Dissipative Living Materials. *J. Am. Chem. Soc.* **2023**, *145*, 1811−1817.
(14) Jo, H.; Sim, S. Programmable Living Materials Constructed with the Dynamic Covalent Interface between Synthetic Polymers and Engineered B. subtilis. *ACS Appl. Mater. Interfaces* **2022**, *14*, 20729−20738.
(15) Setlow, P. Spores of Bacillus subtilis: their resistance to and killing by radiation, heat and chemicals. *J. Appl. Microbiol.* **2006**, *101*, 514−525.
(16) González, L. M.; Mukhitov, N.; Voigt, C. A. Resilient living materials built by printing bacterial spores. *Nat. Chem. Biol.* **2020**, *16*, 126−133.
(17) Hui, Y.; Cui, Z.; Sim, S. Stress-Tolerant, Recyclable, and Renewable Biocatalyst Platform Enabled by Engineered Bacterial Spores. *ACS Synth. Biol.* **2022**, *11*, 2857−2868.
(18) Yesilyurt, V.; Webber, M. J.; Appel, E. A.; Godwin, C.; Langer, R.; Anderson, D. G. Injectable self-healing glucose-responsive hydrogels with pH-regulated mechanical properties. *Adv. Mater.* **2016**, *28*, 86−91.
(19) Ye, Z.; Xiang, Y.; Monroe, T.; Yu, S.; Dong, P.; Xian, S.; Webber, M. J. Polymeric Microneedle Arrays with Glucose-Sensing Dynamic-Covalent Bonding for Insulin Delivery. *Biomacromolecules* **2022**, *23*, 4401−4411.
(20) Ogden, W. A.; Guan, Z. Recyclable, strong, and highly malleable thermosets based on boroxine networks. *J. Am. Chem. Soc.* **2018**, *140*, 6217−6220.
(21) Brooks, W. L.; Sumerlin, B. S. Synthesis and applications of boronic acid-containing polymers: from materials to medicine. *Chem. Rev.* **2016**, *116*, 1375−1397.
(22) Waller, L. N.; Fox, N.; Fox, K. F.; Fox, A.; Price, R. L. Ruthenium red staining for ultrastructural visualization of a glycoprotein layer surrounding the spore of Bacillus anthracis and Bacillus subtilis. *J. Microbiol. Methods* **2004**, *58*, 23−30.
(23) Plomp, M.; Carroll, A. M.; Setlow, P.; Malkin, A. J. Architecture and assembly of the Bacillus subtilis spore coat. *PLoS One* **2014**, *9*, No. e108560.
(24) Bartels, J.; Blüher, A.; López Castellanos, S.; Richter, M.; Günther, M.; Mascher, T. The Bacillus subtilis endospore crust: protein interaction network, architecture and glycosylation state of a potential glycoprotein layer. *Mol. Microbiol.* **2019**, *112*, 1576−1592.
(25) Shuster, B.; Khemmani, M.; Nakaya, Y.; Holland, G.; Iwamoto, K.; Abe, K.; Imamura, D.; Maryn, N.; Driks, A.; Sato, T.; et al. Expansion of the spore surface polysaccharide layer in Bacillus subtilis by deletion of genes encoding glycosyltransferases and glucose modification enzymes. *J. Bacteriol.* **2019**, *201*, No. e00321.
(26) Springsteen, G.; Wang, B. A detailed examination of boronic acid−diol complexation. *Tetrahedron* **2002**, *58*, 5291−5300.
(27) Zarzeczańska, D.; Adamczyk-Woźniak, A.; Kulpa, A.; Ossowski, T.; Sporzyński, A. Fluorinated boronic acids: acidity and hydrolytic stability of fluorinated phenylboronic acids. *Eur. J. Inorg. Chem.* **2017**, *2017*, 4493−4498.
(28) Soundararajan, S.; Duesler, E.; Hageman, J. Structure of 4-carboxy-2-nitrobenzeneboronic acid. *Acta Crystallogr., Sect. C: Cryst. Struct. Commun.* **1993**, *49*, 690−693.
(29) Hammett, L. P. The effect of structure upon the reactions of organic compounds. Benzene derivatives. *J. Am. Chem. Soc.* **1937**, *59*, 96−103.
(30) Brooks, W. L.; Deng, C. C.; Sumerlin, B. S. Structure−reactivity relationships in boronic acid−diol complexation. *ACS Omega* **2018**, *3*, 17863−17870.
(31) Bornscheuer, U. T.; Huisman, G.; Kazlauskas, R.; Lutz, S.; Moore, J.; Robins, K. Engineering the third wave of biocatalysis. *Nature* **2012**, *485*, 185−194.
(32) Hauer, B. Embracing nature's catalysts: a viewpoint on the future of biocatalysis. *ACS Catal.* **2020**, *10*, 8418−8427.

https://doi.org/10.1021/jacs.3c05153
J. Am. Chem. Soc. 2023, 145, 16210−16217